J. Fluid Mech. (2002), *vol.* 464, *pp.* 365–391.
DOI: 10.1017/S0022112002008820 Printed in the United Kingdom

Nonlinear sloshing in zero gravity

By JOHN BILLINGHAM

Department of Mathematics and Statistics, The University of Birmingham, Edgbaston, Birmingham B15 2TT, UK

(Received 17 August 2001 and in revised form 18 February 2002)

We study the effect of a time-periodic, lateral acceleration on the two-dimensional flow of a fluid with a free surface subject to surface tension, confined between two plane, parallel walls under conditions of zero gravity. We assume that the velocity of each contact line is a prescribed, single-valued function of the dynamic contact angle between fluid and solid at the wall. We begin by obtaining analytical solutions for the small-amplitude standing waves that evolve when this function is linear, the fluid is inviscid and the lateral acceleration is sufficiently small. This leads to damping of the motion, unless either the contact angles are fixed or the contact lines are pinned. In these cases, we include the effect on the flow of the wall boundary layers, which are the other major sources of damping. We then consider the weakly nonlinear solution of the inviscid problem when the contact angle is almost constant and the external forcing is close to resonance. This solution indicates the possibility of a hysteretic response to changes in the forcing frequency. Finally, we examine numerical solutions of the fully nonlinear, inviscid problem using a desingularized integral equation technique. We find that periodic solutions, chaotic solutions and solutions where the topology of the fluid changes, either through self-intersection or pinch off, are all possible.

1. Introduction

In a microgravity environment, the motion of fluids is driven by surface tension and external forces. This leads to problems in fluid processing that are rather different to those encountered under normal gravity (for example, Ostrach 1982). One key application where it is crucial to understand the large-amplitude motion of a body of fluid under microgravity conditions is that of a satellite with a partially filled fuel tank. In this case, external forcing is provided by small rockets that are used to orient the satellite. Modelling the details of this fluid/structure interaction is difficult, and the numerical techniques that have been used in previous work are not well suited to capturing the details of the fluid flow close to moving contact lines (see, for example, Gerrits *et al.* 1999). A satellite that will gather experimental data on this problem is due to be launched this year (Gerrits & Veldman 2000).

In order to gain more detailed insight into the response of a body of fluid to external forcing under microgravity conditions, we study a two-dimensional model problem, that of a deep fluid contained between two parallel walls and subject to external, lateral, time-harmonic forcing. We find that the motion of the two contact lines, where the fluid is in contact with both the atmosphere and the solid wall, plays a crucial role in determining the response of the fluid. Kamotani *et al.* (1995) have tackled precisely this problem using a commercial CFD package, but confined their attention to small-amplitude motions at moderate to low Reynolds numbers.

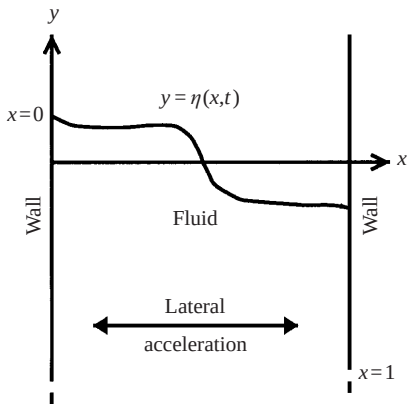

FIGURE 1. The fluid, confining walls and coordinate system.

A closely related problem, that of the settling of an initially disturbed free surface, has previously been tackled by several authors (see Dreyer *et al.* 1998 for a recent review), notably Hocking (1987), who considered the situation under normal gravity, and Weislogel & Ross (1990) and Wölk *et al.* (1997), who discuss the behaviour of a free surface when gravity is suddenly reduced to zero, as occurs in a drop-tower experiment. In each case, the authors consider small-amplitude motions of a free surface, and were able to obtain reasonably good agreement with experiment. We shall discuss some aspects of their work in more detail later.

After setting up the governing equations for our model problem in § 2, we begin by studying the standing waves that are generated by small-amplitude forcing in § 3. In § 3.1 we examine large-Reynolds-number standing wave solutions. We find that the effect of viscosity will be important in boundary layers at the walls when either the contact angles are fixed or the contact lines are pinned, and study these cases in §§ 3.2 and 3.3. In § 4, we perform a weakly nonlinear analysis of the inviscid problem for forcing close to a resonant frequency when the contact angles are almost constant. Finally, in § 5, we study the fully nonlinear, inviscid problem using a desingularized integral equation method, after using the analytical solutions that we have obtained to validate this numerical technique.

2. The initial value problem

We consider the two-dimensional motion of a Newtonian fluid in a parallel-sided container, as illustrated in figure 1, which also shows the (x, y)-coordinate system. The depth of the fluid is sufficient that it can be assumed infinite. The fluid has a free surface, with surface tension. At each contact line, the contact line velocity is assumed to be a prescribed, single-valued function of the dynamic contact angle. There is no background gravitational field, but the fluid undergoes a time-periodic acceleration in the lateral (x) direction. This can be thought of as due either to lateral shaking of the container, or to a weak, oscillatory, background gravitational field, as can exist on spacecraft (g-jitter). The velocity and pressure fields in the fluid are $\boldsymbol{u}(x, y, t)$ and $p(x, y, t)$, and the free surface lies at $y = \eta(x, t)$. We work in terms of dimensionless variables, with length, time, velocity and pressure scaled with a, $(\rho a^3/\sigma)^{1/2}$, $(\sigma/a\rho)^{1/2}$ and σ/a respectively, where a is the lateral extent of the container, and ρ and σ are the density and surface tension of the fluid.

The dimensionless governing equations are

$$\frac{\partial \boldsymbol{u}}{\partial t} + \boldsymbol{u}\cdot\nabla\boldsymbol{u} = -\nabla p + Bo\,\sin\omega t\nabla x + Re^{-1}\nabla^2\boldsymbol{u}, \quad \nabla\cdot\boldsymbol{u} = 0$$

$$\text{for} \quad 0 \leqslant x \leqslant 1, \quad y \leqslant \eta(x,t), \quad t \geqslant 0, \tag{2.1}$$

to be solved subject to

$$\frac{\partial \eta}{\partial t} + u_x\frac{\partial \eta}{\partial x} = u_y, \tag{2.2}$$

$$p = -\frac{\partial^2\eta}{\partial x^2}\left\{1+\left(\frac{\partial\eta}{\partial x}\right)^2\right\}^{-3/2} + \frac{2Re^{-1}}{1+(\partial\eta/\partial x)^2}\left[\left\{\left(\frac{\partial\eta}{\partial x}\right)^2 - 1\right\}\frac{\partial u_x}{\partial x} - \frac{\partial\eta}{\partial x}\left(\frac{\partial u_x}{\partial y}+\frac{\partial u_y}{\partial x}\right)\right], \tag{2.3}$$

$$\frac{Re^{-1}}{1+\left(\partial\eta/\partial x\right)^2}\left[\left\{1-\left(\frac{\partial\eta}{\partial x}\right)^2\right\}\left(\frac{\partial u_x}{\partial y}+\frac{\partial u_y}{\partial x}\right) - 4\frac{\partial\eta}{\partial x}\frac{\partial u_x}{\partial x}\right] = 0, \tag{2.4}$$

at $y = \eta(x,t)$ for $0 \leqslant x \leqslant 1$, where $\boldsymbol{u} = (u_x, u_y)$, and

$$\boldsymbol{u} = 0 \quad \text{at} \quad x = 0 \quad \text{and} \quad x = 1, \tag{2.5}$$

$$\boldsymbol{u} \to 0 \quad \text{as} \quad y \to -\infty, \tag{2.6}$$

$$\boldsymbol{u} = 0, \quad \eta = \eta_i(x) \quad \text{when} \quad t = 0, \tag{2.7}$$

where $\eta_i(x)$ is the initial displacement of the free surface. The fluid is stationary when $t = 0$. The contact line boundary condition is

$$\frac{\partial\eta}{\partial t} = \begin{cases} C\left(\dfrac{\partial\eta}{\partial x}\right) & \text{at} \quad x = 0, \\ C\left(-\dfrac{\partial\eta}{\partial x}\right) & \text{at} \quad x = 1, \end{cases} \tag{2.8}$$

where $C(.)$ is some prescribed function. The dimensionless parameters are

$$Re = \left(\frac{\rho a\sigma}{\mu^2}\right)^{1/2}, \quad Bo = \frac{\rho a^2 A\omega_0^2}{\sigma}, \quad \omega = \left(\frac{\rho a^3}{\sigma}\right)^{1/2}\omega_0, \tag{2.9}$$

the Reynolds number, Bond number and dimensionless frequency respectively, where ω_0 and A are the frequency and amplitude of the lateral excitation. Note that Re^{-1} is often referred to as the Ohnesorge number, Oh. We will assume that $Re \gg 1$, so that the fluid is inviscid at leading order outside the boundary layers. For water, $Re \approx 8000a^{1/2}$ when a is measured in metres, so we need the container to be wider than about 10^{-3} m for this approximation to be valid.

We impose a no-slip boundary condition along each wall of the container. It is well-known (Dussan V. & Davis 1974) that this leads to a physically unacceptable singularity in the velocity gradient at the contact line, and hence to a singular force there, unless the contact line is either pinned or meets the wall at a tangent. This difficulty can be dealt with mathematically by postulating that the fluid slips at the wall in some small neighbourhood of the contact line. If this neighbourhood

is sufficiently small, viscous forces cause the free surface to bend through an $O(1)$ angle close to the wall, so that the limiting contact angle as the contact line is approached from the bulk of the fluid (the apparent contact angle) is different from the microscopic, or actual contact angle (Cox 1986, 1998). We can therefore think of the function $C(\partial\eta/\partial x)$ as specifying the dependence of the inner limit of the outer solution – the apparent contact angle. It is usual to think of this as changing as the outer flow develops, whilst the microscopic contact angle remains constant. Another interpretation is available using the theory of Shikhmurzaev (1993), in which, although the region where the fluid slips at the wall is not small enough that viscous bending affects the contact angle at leading-order, the *microscopic* contact angle varies as a function of the flow, due to surface tension relaxation effects. We will not consider the details of how the contact line singularity is to be resolved in this paper. One consequence of this is that the viscous correction to the leading-order deformation of the free surface is logarithmically singular as $x \to 0$ and $x \to 1$. This means that, in the following calculations, any correction term in an expansion for some property of the flow that depends upon the viscous correction term in the expansion of the contact line condition (2.8) is dependent upon the detailed resolution of the contact line singularity. We regard such corrections as beyond the scope of the present paper.

In this paper, we will assume that

$$C\left(\frac{\partial\eta}{\partial x}\right) = \lambda\frac{\partial\eta}{\partial x}, \tag{2.10}$$

so that the contact line velocity varies linearly with the slope at the contact line, and the static contact angle is $\pi/2$. In particular, the speed of the contact line tends to infinity as the contact angle tends to zero or π. It is unlikly that this is precisely the correct model for any given fluid/solid combination, but it is also clear that there is, as yet, no universally accepted model of the form (2.8) that we can use. As we have discussed above, θ_c is the apparent contact angle – the outer limit of the inner solution close to the contact line, where viscosity is important, and we have yet to attempt to solve the inner problem. In addition, there is no agreement on the dependence of the actual dynamic contact angle on the contact line velocity, although many models have been proposed (see Shikhmurzaev 1993 for a review of these, along with a new model). The simple model, (2.10), which we use here, should be seen as a reasonable estimate of the actual behaviour, and our results give us some idea of the qualitative behaviour for large-amplitude displacements of the free surface. Of course, for small-amplitude motions, with which much of this paper is concerned, (2.10) is equivalent to the linearized form of (2.8), whatever model is used.

We begin by studying the linearized version of the problem. We expect that this will be appropriate when $Bo \ll 1$. As we shall see, it is possible to make considerable analytical progress on this problem, since the domain of solution for the linearized problem is a semi-infinite strip. We would not expect the *qualitative* nature of the solution to change for static contact angles moderately different from $\pi/2$. The boundary condition (2.10) was also used by Hocking (1987) in his analysis of the unforced response of this system. Kamotani *et al.* (1995) and Wölk *et al.* (1997) used a similar boundary condition valid for an arbitrary static contact angle, but with the dynamic contact angle a linear function of the *displacement* of the free surface rather than its velocity. Although this is hard to justify on physical grounds, it is equivalent to (2.10) for the small-amplitude, time-harmonic motions that they were studying.

3. Standing wave solutions for forcing of small amplitude

In this section, we consider what happens when the external forcing is of small amplitude. These analytical results are of interest in themselves, and also provide a good test of the numerical solution method that we describe in § 5. Although it is possible to scale the Bond number, Bo, out of the problem, to avoid confusion we will not do this, since we will need to assume in §§ 3.2 and 3.3 that $Bo = O(Re^{-1/2})$. Of course, this means that we should expect the deformation of the free surface to be proportional to Bo in the following calculations.

At leading order, for deformations of the free surface of sufficiently small amplitude, (2.1)–(2.7) become

$$\frac{\partial \boldsymbol{u}}{\partial t} = -\nabla p + Bo\, \sin \omega t \nabla x + Re^{-1}\nabla^2 \boldsymbol{u}, \quad \nabla \cdot \boldsymbol{u} = 0$$
$$\text{for} \quad 0 \leqslant x \leqslant 1, \quad y \leqslant 0, \quad t \geqslant 0, \tag{3.1}$$

to be solved subject to

$$\frac{\partial \eta}{\partial t} = u_y, \quad p = -\frac{\partial^2 \eta}{\partial x^2} - 2Re^{-1}\frac{\partial u_x}{\partial x}, \quad Re^{-1}\left(\frac{\partial u_x}{\partial y} + \frac{\partial u_y}{\partial x}\right) = 0 \quad \text{at} \quad y = 0, \tag{3.2a–c}$$

and

$$\boldsymbol{u} = 0 \quad \text{at} \quad x = 0 \quad \text{and} \quad x = 1, \tag{3.3}$$
$$\boldsymbol{u} \to 0 \quad \text{as} \quad y \to -\infty, \tag{3.4}$$
$$\boldsymbol{u} = 0, \quad \eta = 0 \quad \text{when} \quad t = 0. \tag{3.5}$$

For simplicity, we will only consider the standing wave driven by the lateral forcing, which will be the leading-order solution of this linear problem for $t \gg 1$ once the initial transients have decayed. Note that this standing wave is antisymmetric about the line $x = 1/2$. We pose asymptotic expansions

$$\left.\begin{aligned} \boldsymbol{u} = \boldsymbol{u}_0 + Re^{-1/2}\boldsymbol{u}_1 + o(Re^{-1/2}), \quad p = p_0 + Re^{-1/2}p_1 + o(Re^{-1/2}), \\ \eta = \eta_0 + Re^{-1/2}\eta_1 + o(Re^{-1/2}), \end{aligned}\right\} \tag{3.6}$$

for $Re \gg 1$, and substitute into (3.1)–(3.5). At leading order, the pressure is harmonic, and is given by

$$p_0 = Bo\, \sin \omega t \left(x - \tfrac{1}{2}\right) + \sum_{n=1}^{\infty} B_n(t) \cos(2n-1)\pi x\, \mathrm{e}^{(2n-1)\pi y}, \tag{3.7}$$

with the functions $B_n(t)$ to be determined. The dynamic boundary condition, (3.2b), at leading order, when integrated twice, gives

$$\eta_0 = -\tfrac{1}{6}Bo\, \sin \omega t (x - \tfrac{1}{2})^3 + B_0(t)(x - \tfrac{1}{2}) + \sum_{n=1}^{\infty} \frac{1}{(2n-1)^2\pi^2} B_n(t) \cos(2n-1)\pi x. \tag{3.8}$$

Note that we can express the linear term as a Fourier series, using

$$x - \tfrac{1}{2} = -4 \sum_{n=1}^{\infty} \frac{1}{(2n-1)^2\pi^2} \cos(2n-1)\pi x. \tag{3.9}$$

We must, however, take care, since the derivative of this series is not everywhere constant, but includes a periodic sequence of delta functions located at the walls,

because the function that the series represents is periodic and only piecewise linear. Similar comments apply to the Fourier series expansion of the cubic term in (3.8). In particular, we now apply the contact line condition, (2.8), at leading order, and calculate the slope at $x = 0$ on the assumption that the function whose Fourier series appears in (3.8) has zero slope at the origin, so that the slope is given by the algebraic terms alone in (3.8). As a consequence, we must have

$$B_n \to 0 \quad \text{as} \quad n \to \infty. \tag{3.10}$$

We find that

$$B_0 = \tfrac{1}{8} Bo \sin \omega t + \frac{1}{\lambda} \left\{ \sum_{m=1}^{\infty} \frac{1}{(2m-1)^2 \pi^2} \frac{\partial B_m}{\partial t} - \frac{1}{2} \frac{\partial B_0}{\partial t} + \tfrac{1}{48} Bo\, \omega \cos \omega t \right\}. \tag{3.11}$$

The kinematic condition, (3.2a), gives, equating coefficients of $\cos(2n-1)\pi x$ at leading order,

$$\frac{\partial^2 B_n}{\partial t^2} + \omega_{2n-1}^2 B_n = 4 \frac{\partial^2 B_0}{\partial t^2} - \frac{1}{2} \left\{ \frac{8}{(2n-1)^2 \pi^2} - 1 \right\} Bo\, \omega^2 \sin \omega t, \tag{3.12}$$

where

$$\omega_m^2 = m^3 \pi^3. \tag{3.13}$$

We can combine (3.11) and (3.12) by defining $\hat{B}_n$ through

$$B_n = 4B_0 + (2n-1)^2 \pi^2 \hat{B}_n, \tag{3.14}$$

so that

$$\frac{\partial^2 \hat{B}_n}{\partial t^2} + \omega_{2n-1}^2 \hat{B}_n = \frac{1}{(2n-1)^2 \pi^2} \left\{ \tfrac{1}{2} (\omega^2 - \omega_{2n-1}^2) - \frac{4\omega^2}{(2n-1)^2 \pi^2} \right\} Bo \sin \omega t$$
$$- \frac{4(2n-1)\pi}{\lambda} \left(\sum_{m=1}^{\infty} \frac{\partial \hat{B}_m}{\partial t} + \tfrac{1}{48} Bo\, \omega \cos \omega t \right), \tag{3.15}$$

whilst

$$p_0 = Bo(x - \tfrac{1}{2}) \sin \omega t + \sum_{n=0}^{\infty} \{ (2n-1)^2 \pi^2 \hat{B}_n + 4B_0 \} \cos(2n-1)\pi x\, \mathrm{e}^{(2n-1)\pi y}. \tag{3.16}$$

The time-harmonic solutions of the unforced version of (3.15) were studied by Hocking (1987), who made the substitution $\hat{B}_n = b_n \mathrm{e}^{\mathrm{i}\omega t}$ when $Bo = 0$. He showed that there is a sequence of resonant frequencies, $\omega = \Omega_m$, which are complex for $0 < \lambda < \infty$, and are given by the solutions of

$$\sum_{n=1}^{\infty} \frac{2n-1}{\omega_{2n-1}^2 - \Omega_m^2} + \frac{\lambda}{4\pi \mathrm{i} \Omega_m} = 0. \tag{3.17}$$

When $\lambda = 0$ (pinned contact lines) or $\lambda = \infty$ (fixed contact angles), the resonant frequencies of the system are real, and we conclude that the contact lines provide no damping of the motion. In these cases, if the excitation is at one of the resonant frequencies, the solution grows linearly with time. We therefore consider these two situations separately below, and include the effect of the viscous boundary layers on the solid walls, since they are then the main source of damping. In contrast, unless λ is either sufficiently large or sufficiently small (we will quantify this later), the motion

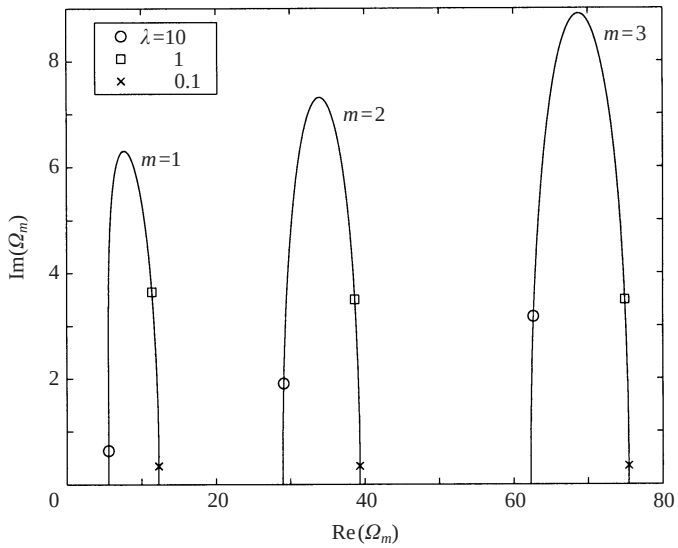

FIGURE 2. The three resonant frequencies with the smallest real parts, Ω_1, Ω_2 and Ω_3, obtained from (3.17). The points at which $\lambda = 0.1$, 1 and 10 are marked. Each frequency changes monotonically with λ and is real when $\lambda = 0$ or ∞.

of the contact lines is the dominant source of damping of the fluid motion. The three resonant frequencies with the smallest real parts, Ω_1, Ω_2 and Ω_3, are plotted in figure 2.

3.1. *Solution for* $0 < \lambda < \infty$

In order to determine the standing wave excited by the lateral forcing, we simply seek a solution of the form

$$\hat{B}_n = R_n \, \mathrm{e}^{\mathrm{i}\omega t}. \tag{3.18}$$

Since the unforced system is damped, we know that R_n must be bounded. We find that the deformation of the free surface is given by

$$\eta(x,t) = \mathrm{e}^{\mathrm{i}\omega t} \sum_{n=1}^{\infty} \hat{R}_n \cos(2n-1)\pi x, \tag{3.19}$$

where

$$\hat{R}_n = \frac{Bo}{\omega_{2n-1}^2 - \omega^2} \left\{ \frac{4\mathrm{i}}{(2n-1)\pi} + \frac{4(2n-1)\pi\omega}{\lambda + 4\mathrm{i}\omega S_1} (4\omega^2 S_2 + \tfrac{1}{24}) \right\}, \tag{3.20}$$

and

$$S_1 = \sum_{m=1}^{\infty} \frac{(2m-1)\pi}{\omega_{2m-1}^2 - \omega^2}, \quad S_2 = \sum_{m=1}^{\infty} \frac{1}{(2m-1)^4\pi^4(\omega_{2m-1}^2 - \omega^2)}. \tag{3.21}$$

Note that the limiting value of this expression as $\omega \to \omega_{2m-1}$ is well-defined. Figure 3 shows the maximum amplitude of the standing wave solution as a function of ω for $\lambda = 0.1$, 1 and 10. This should be compared with figure 2, which shows the resonant frequencies of the system. As we would expect, the maximum amplitude of the standing wave has local maxima in the neighbourhood of the real part of the resonant frequencies.

In the work of Kamotani *et al.* (1995), the dimensionless deformation of the free

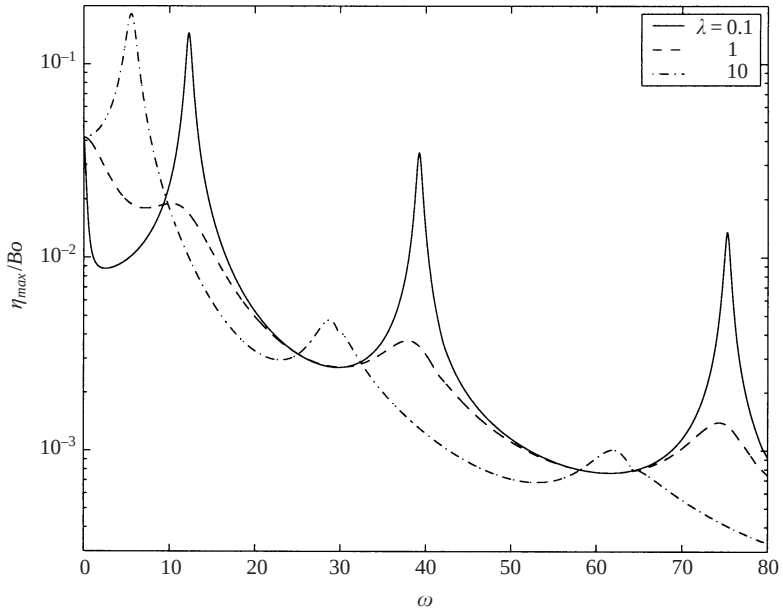

FIGURE 3. The maximum amplitude of the standing wave solution for $\lambda = 0.1$, 1 and 10.

surface is everywhere less that 0.015, which, at first sight means that their results should be directly comparable to ours. However, their results are for rather small Reynolds numbers ($Re < 200$), and we find that their free-surface deformations are somewhat smaller than those that we predict, presumably due to the effect of viscosity in both the bulk fluid and the surface boundary layer, which we neglect. The authors themselves state that they were unable to resolve the boundary layers numerically for larger values of the Reynolds number. In addition, their method of dealing with the stress singularity at the contact lines is unclear.

3.2. *Fixed contact angles* ($\lambda = \infty$)

As we shall see below, the presence of boundary layers on the walls of the container leads to a correction to the outer flow at $O(Re^{-1/2})$. This means that, when the lateral excitation is at one of the resonant frequencies, we need to assume that $Bo = O(Re^{-1/2})$ for the standing wave that it excites to be of $O(1)$ as $Re \to \infty$. We therefore define

$$\overline{Bo} = Re^{1/2} Bo, \tag{3.22}$$

with $\overline{Bo} = O(1)$. At leading order, (3.11) and (3.15) now show that $B_0 = 0$ and

$$\frac{\partial^2 \hat{B}_n}{\partial t^2} + \omega_{2n-1}^2 \hat{B}_n = 0. \tag{3.23}$$

The resonant frequencies of the system are therefore ω_{2n-1} at leading order.

At this point, we make a small diversion to consider the solution of the unforced, inviscid problem,

$$\eta = \sum_{n=1}^{\infty} \hat{B}_{n0} \cos \omega_{2n-1} t \cos(2n-1)\pi x, \tag{3.24}$$

where the constants $\hat{B}_{n0}$ are determined by the Fourier components of a non-zero

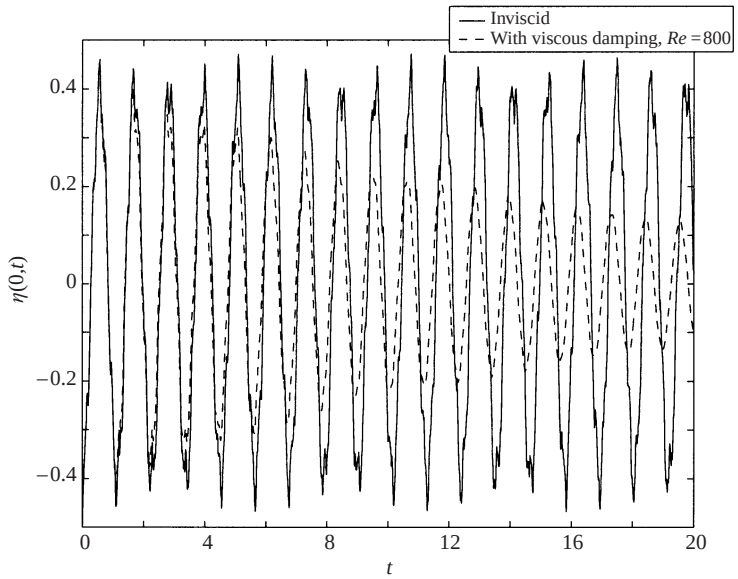

FIGURE 4. The position of the contact line when $\eta(x,0) = x - \frac{1}{2}$, for a fixed contact angle ($\lambda = \infty$). The broken line shows the effect of viscous damping when $Re = 800$.

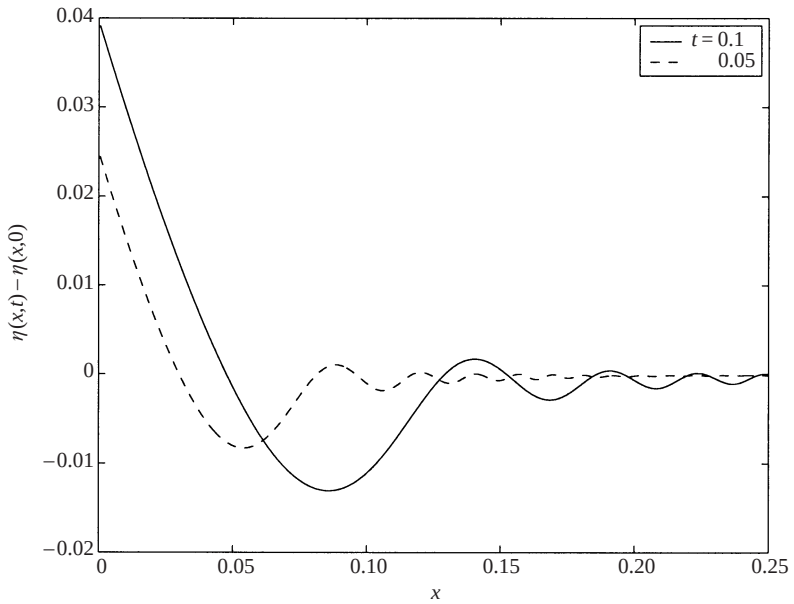

FIGURE 5. The initial motion of the free surface close to the contact line when $\eta(x,0) = x - \frac{1}{2}$, for a fixed contact angle ($\lambda = \infty$).

initial displacement of the free surface. The position of the contact line at $x = 0$ is shown in figure 4 for $\eta(x,0) = x - \frac{1}{2}$. The jaggedness of the motion is striking, and is a fully reproducible feature of the flow, arising from the form of the analytical solution, (3.24). The initial motion of the contact line as the slope of the free surface adjusts from the initial contact angle to $\partial\eta/\partial x = 0$ is violent, and locally given by the similarity solution studied by Billingham & King (1995), where lengths scale on $t^{2/3}$.

This is illustrated in figure 5, which shows capillary waves propagating away from the contact line, in agreement with figure 3 of Billingham & King (1995). Once the waves generated at each of the contact lines begin to interact, the irregular motion sets in. It is also straightforward to include the effect of the damping due to the boundary layers on the walls using the results given by Hocking (1987), so that

$$\eta = \sum_{n=1}^{\infty} \hat{B}_{n0} \exp\left\{-\left(\frac{\omega_{2n-1}}{2Re}\right)^{1/2} t\right\} \cos\left\{\omega_{2n-1} + \left(\frac{\omega_{2n-1}}{2Re}\right)^{1/2}\right\} t \cos(2n-1)\pi x. \quad (3.25)$$

For water between walls 1 cm apart, $Re \approx 800$, and this case is also shown in figure 4. Note that the time scale is approximately 0.12 s.

Returning now to consider the effect of the lateral excitation, we assume that $\omega = \omega_{2N-1}$, and seek a standing wave solution

$$\hat{B}_n = \begin{cases} \bar{B}_N \exp(\mathrm{i}\omega_{2N-1} t) & \text{for} \quad n = N, \\ 0 & \text{for} \quad n \neq N. \end{cases} \quad (3.26)$$

In the following, all variables are understood to have time dependence of the form $\exp(\mathrm{i}\omega_{2N-1}t)$. We note that neither (3.2*c*), no shear stress on the free surface, nor the y-component of (3.3), the no-slip boundary condition, are satisfied by the leading-order solution, which has

$$u_{x0} = -\mathrm{i}\omega_{2N-1}\bar{B}_N \sin(2N-1)\pi x \, \mathrm{e}^{(2N-1)\pi y}, \quad (3.27)$$

$$u_{y0} = \mathrm{i}\omega_{2N-1}\bar{B}_N \cos(2N-1)\pi x \, \mathrm{e}^{(2N-1)\pi y}. \quad (3.28)$$

This means that there must be boundary layers at the walls and the free surface, across which these boundary conditions are satisfied. The free-surface boundary layer is asymptotically weaker than those at the walls, and we will not consider it here. We define scaled boundary layer variables

$$\hat{x} = Re^{1/2}x, \quad \hat{u}_{x0} = Re^{1/2}u_{x0}, \quad (3.29)$$

with $\hat{x}$, $\hat{u}_{x0} = O(1)$ as $Re \to \infty$. In terms of these, the leading-order problem in the boundary layer at $x = 0$ is

$$\frac{\partial p_0}{\partial \hat{x}} = 0, \quad \mathrm{i}\omega_{2N-1}u_{y0} = -\frac{\partial p_0}{\partial y} + \frac{\partial^2 u_{y0}}{\partial \hat{x}^2}, \quad \frac{\partial u_{y0}}{\partial y} + \frac{\partial \hat{u}_{x0}}{\partial \hat{x}} = 0, \quad (3.30)$$

subject to

$$u_{y0} = \hat{u}_{x0} = 0 \quad \text{at} \quad \hat{x} = 0, \quad (3.31)$$

$$p_0 \sim (2N-1)^2\pi^2\bar{B}_N \, \mathrm{e}^{(2N-1)\pi y} \quad \text{as} \quad \hat{x} \to \infty, \quad (3.32)$$

$$\hat{u}_{y0} \sim \mathrm{i}\omega_{2N-1}\bar{B}_N \, \mathrm{e}^{(2N-1)\pi y} \quad \text{as} \quad \hat{x} \to \infty. \quad (3.33)$$

At leading order, the pressure, p_0, does not change across the boundary layer, and is given by (3.32), whilst the solution for the fluid velocity is

$$u_{y0} = \mathrm{i}\omega_{2N-1}\bar{B}_N \, \mathrm{e}^{(2N-1)\pi y}\{1 - \exp(-(\mathrm{i}\omega_{2N-1})^{1/2}\hat{x})\}, \quad (3.34)$$

$$\hat{u}_{x0} = \mathrm{i}\omega_{2N-1}(2N-1)\pi\bar{B}_N \, \mathrm{e}^{(2N-1)\pi y}\left\{\frac{1 - \exp(-(\mathrm{i}\omega_{2N-1})^{1/2}\hat{x})}{(\mathrm{i}\omega_{2N-1})^{1/2}} - \hat{x}\right\}. \quad (3.35)$$

As $\hat{x} \to \infty$ in (3.35), the term linear in $\hat{x}$ matches with the outer solution, (3.27). The term independent of $\hat{x}$ drives a term of $O(Re^{-1/2})$ in the outer flow through the

boundary condition

$$u_{x1} = (\mathrm{i}\omega_{2N-1})^{1/2}(2N-1)\pi\bar{B}_N\,\mathrm{e}^{(2N-1)\pi y} \quad \text{at} \quad x = 0, 1, \tag{3.36}$$

using the antisymmetry of the flow, and hence

$$\frac{\partial p_1}{\partial x} = -(\mathrm{i}\omega_{2N-1})^{3/2}(2N-1)\pi\bar{B}_N\,\mathrm{e}^{(2N-1)\pi y} + \mathrm{i}\overline{Bo} \quad \text{at} \quad x = 0, 1. \tag{3.37}$$

Now, considering the other component of velocity, we can write a composite solution for u_{y0} as

$$u_{y0} = \mathrm{i}\omega_{2N-1}\bar{B}_N\,\mathrm{e}^{(2N-1)\pi y}\{\cos(2N-1)\pi x - \exp(-(\mathrm{i}\omega_{2N-1}Re)^{1/2}x) + \exp(-(\mathrm{i}\omega_{2N-1}Re)^{1/2}(1-x))\}. \tag{3.38}$$

If we extract the appropriate Fourier component from the difference of the two exponentials in (3.38), we find that

$$u_{y0} = \mathrm{i}\omega_{2N-1}\bar{B}_N\,\mathrm{e}^{(2N-1)\pi y}\left\{1 - \frac{4}{(\mathrm{i}\omega_{2N-1}Re)^{1/2}}\right\}\cos(2N-1)\pi x. \tag{3.39}$$

The boundary layer therefore leads to a contribution to the y-component of the velocity of $O(Re^{-1/2})$, which we need to include in the kinematic boundary condition at that order, so that

$$\frac{\partial p_1}{\partial y} = \omega_{2N-1}^2\eta_1 - 4(\mathrm{i}\omega_{2N-1})^{3/2}\bar{B}_N\cos(2N-1)\pi x \quad \text{at} \quad y = 0. \tag{3.40}$$

Finally, the equation for the pressure and the dynamic boundary condition at $O(Re^{-1/2})$ are

$$\nabla^2 p_1 = 0, \tag{3.41}$$

$$p_1 = -\frac{\partial^2\eta_1}{\partial x^2} \quad \text{at} \quad y = 0. \tag{3.42}$$

Now, if we had to solve for η_1, we would run into the difficulty, associated with the singularity at the contact line, that η_1 is logarithmically singular as $x \to 0$ and $x \to 1$, which we discussed in § 2. However, when determining the viscous contribution to the rate of damping, Mei & Liu (1973) and Hocking (1987) showed that the divergence theorem, along with the antisymmetry of the flow, can be used to determine $\bar{B}_N$ without solving for η_1. In particular,

$$\int_0^1\int_{-\infty}^0 (p_0\nabla^2 p_1 - p_1\nabla^2 p_0)\,\mathrm{d}y\,\mathrm{d}x = \int_0^1 \left(p_0\frac{\partial p_1}{\partial y} - p_1\frac{\partial p_0}{\partial y}\right)\bigg|_{y=0}\mathrm{d}x - 2\int_{-\infty}^0 \left(p_0\frac{\partial p_1}{\partial x} - p_1\frac{\partial p_0}{\partial x}\right)\bigg|_{x=0}\mathrm{d}y = 0. \tag{3.43}$$

The key points are that, since $\partial p_0/\partial x = 0$ at $x = 0$, we do not need to know p_1 there, and that once (3.16), (3.37), (3.40) and (3.42) have been substituted into (3.43), the terms in η_1 cancel out after integration by parts. Note that this cancellation does not occur if we attempt to determine the form of this resonant solution in more detail by assuming that $\lambda^{-1} = O(Re^{-1/2})$. The solution must therefore then be dependent upon the precise mechanism by which the no-slip boundary condition is modified close to the contact line, and we will not consider this further here.

After some algebra, we find that the amplitude of the standing wave is

$$\bar{B}_N = \frac{2\mathrm{e}^{\pi \mathrm{i}/4}\overline{Bo}}{(2N-1)^{13/4}\pi^{13/4}}. \tag{3.44}$$

This amplitude decreases rapidly with N, with $|\bar{B}_1|/|\bar{B}_2| \approx 35.5$. The mode most likely to be excited is therefore that with $N = 1$, a sloshing motion with $\eta \propto \cos \pi x$ and amplitude

$$|\bar{B}_1| = \frac{2\overline{Bo}}{\pi^{13/4}} \approx 0.048\overline{Bo}. \tag{3.45}$$

The small numerical coefficient in this expression means that our linearization of the whole problem is valid provided that $0.048\overline{Bo}$ is small. We can now determine how large λ can be, for a given value of the Reynolds number, before viscosity is no longer negligible. When $\lambda = \infty$, the resonant frequencies are ω_{2n-1}. For λ large but finite, if $\omega = \omega_{2N-1}$, we find from (3.20) that

$$\eta \sim -\frac{\lambda Bo}{(2N-1)^{7/2}\pi^{7/2}} \cos(2N-1)\pi x. \tag{3.46}$$

Comparing this with (3.44), we find that the maximum value of η for $\lambda \gg 1$ in the absence of viscosity is comparable to the maximum value of η when $\lambda = \infty$ with viscosity present when

$$\lambda = O(2Re^{1/2}(2N-1)^{1/4}\pi^{1/4}). \tag{3.47}$$

For the mode with the lowest frequency, $N = 1$, this occurs when $\lambda = O(2.6Re^{1/2})$. For water with walls 1 cm apart, $2.6Re^{1/2} \approx 75$.

3.3. *Pinned contact lines with viscosity* ($\lambda = 0$)

In this case, the leading-order equations are

$$\sum_{m=1}^{\infty} \frac{\partial \hat{B}_m}{\partial t} = 0, \tag{3.48}$$

$$\frac{\partial^2 \hat{B}_n}{\partial t^2} + \omega_{2n-1}^2 \hat{B}_n = (2n-1)\left(\frac{\partial^2 \hat{B}_1}{\partial t^2} + \omega_1^2 \hat{B}_1\right). \tag{3.49}$$

These have solutions of the form

$$\hat{B}_n = K_{n0} + \sum_{m=1}^{\infty} K_{nm} \exp(\mathrm{i}\Omega_m t), \tag{3.50}$$

where Ω_m are the resonant frequencies of the system. Equation (3.17) shows that these are real, and solutions of

$$\sum_{n=1}^{\infty} \frac{2n-1}{\omega_{2n-1}^2 - \Omega_m^2} = 0. \tag{3.51}$$

In addition, the coefficients satisfy

$$K_{n0} = \frac{1}{(2n-1)^2\pi^2} K_{10}, \quad K_{nm} = \frac{(2n-1)(\omega_1^2 - \Omega_m^2)}{\omega_{2n-1}^2 - \Omega_m^2} K_{1m}. \tag{3.52}$$

The time-independent part of the solution for the free surface is therefore just a straight line between the two points where it is pinned at the walls, determined by

the initial conditions. We seek the standing wave solution in the resonant case, when $\omega = \Omega_M$, in the form

$$\hat{B}_n = \frac{1}{(2n-1)^2\pi^2}K_0 + \frac{(2n-1)\pi}{\omega_{2n-1}^2 - \Omega_M^2}K_M \exp(\mathrm{i}\Omega_M t). \tag{3.53}$$

We proceed exactly as we did in the previous section, although the algebra is slightly more involved since we must retain the full Fourier series representation of the solution. In particular, we note that

$$B_n = (2n-1)^2\pi^2\hat{B}_n + 4B_0 = K_0 + \frac{\omega_{2n-1}^2}{\omega_{2n-1}^2 - \Omega_M^2}K_M \exp(\mathrm{i}\Omega_M t) + 4B_0. \tag{3.54}$$

Now, in order to be consistent with (3.10), we must have

$$B_0 = -\tfrac{1}{4}K_0 - \tfrac{1}{4}K_M \exp(\mathrm{i}\Omega_M t), \quad B_n = \frac{\Omega_M^2}{\omega_{2n-1}^2 - \Omega_M^2}K_M \exp(\mathrm{i}\Omega_M t), \tag{3.55}$$

and hence

$$p_0 = -K_M \exp(\mathrm{i}\Omega_M t)\sum_{n=1}^{\infty} \frac{\Omega_M^2}{\omega_{2n-1}^2 - \Omega_M^2}\cos(2n-1)\pi x\, \mathrm{e}^{(2n-1)\pi y}. \tag{3.56}$$

We can now proceed without difficulty, and find that

$$K_M = \mathrm{e}\, u^{\pi\mathrm{i}/4}\overline{Bo}\sum_{n=1}^{\infty}\frac{1}{(2n-1)\pi(\omega_{2n-1}^2 - \Omega_M^2)}$$

$$\times\Omega_M^{-3/2}\left[\sum_{n=1}^{\infty}\frac{(2n-1)\pi}{(\omega_{2n-1}^2 - \Omega_M^2)^2} + \int_{-\infty}^{0}\left\{\sum_{n=1}^{\infty}\frac{(2n-1)\pi}{\omega_{2n-1}^2 - \Omega_M^2}\,\mathrm{e}^{(2n-1)\pi y}\right\}^2 \mathrm{d}y\right]^{-1}. \tag{3.57}$$

This gives

$$|K_1| \approx 0.197\overline{Bo}, \quad |K_2| \approx 0.047\overline{Bo}, \tag{3.58}$$

so that, as for the case of a fixed contact angle, the lowest-frequency standing wave is the one most likely to be observed. However, in this case $|K_1|/|K_2| \approx 4.2$, so this tendency is not as marked as for the fixed contact angle. In addition, for fixed values of the Bond and Reynolds numbers, the amplitude of the lowest-frequency standing wave is somewhat larger for the pinned contact line than for the fixed contact angle, and hence the maximum Bond number for which our linearization of the problem is appropriate is somewhat smaller. Although this seems rather counter-intuitive at first sight, the pinned contact line does not generate a net flow along the boundary layers, so we might expect that the consequent rate of damping would be lower. This is consistent with Hocking's (1987) results.

We can now determine how small λ can be, for a given value of the Reynolds number, before viscosity is no longer negligible. When $\lambda = 0$, the resonant frequencies are Ω_m, the solutions of (3.17). For λ small but non-zero, with $\omega = \Omega_M$, we find from (3.20) that

$$\hat{R}_n \sim \frac{4(2n-1)\pi Bo\,\Omega_M}{\lambda(\omega_{2n-1}^2 - \Omega_M^2)}\left\{\frac{1}{24} + 4\Omega_M^2\sum_{m=1}^{\infty}\frac{1}{(2m-1)^4\pi^4(\omega_{2m-1}^2 - \Omega_M^2)}\right\}. \tag{3.59}$$

For the mode with the lowest frequency, $\Omega_1 \approx 12.26$, this gives

$$\eta_{max} \sim \frac{1.45 \times 10^{-2}}{\lambda} Bo. \tag{3.60}$$

At the same frequency, we find that the maximum value of η when $\lambda = 0$ with viscosity present is

$$\eta_{max} \sim 5.86 \times 10^{-3} \overline{Bo}. \tag{3.61}$$

Note that this is ten times smaller than the amplitude of the oscillation when $\lambda = \infty$, given by (3.45). The amplitudes given by (3.60) and (3.61) are comparable when $\lambda = O(2.47Re^{-1/2})$. For water with walls 1 cm apart, $2.47Re^{-1/2} \approx 8.8 \times 10^{-2}$.

4. Weakly nonlinear, inviscid solution for almost fixed contact angles, close to resonance

Following the procedure used by Ockendon & Ockendon (1973), we find that appropriate scaled variables for analysing the weakly nonlinear irrotational sloshing of an inviscid fluid when $Bo \ll 1$ are

$$\hat{\phi} = Bo^{-1/3}\phi, \quad \hat{\eta} = Bo^{-1/3}\eta,$$

with $\hat{\phi}$, $\hat{\eta} = O(1)$ as $Bo \to 0$, where ϕ is the velocity potential, and $\boldsymbol{u} = \nabla\phi$. We also need the contact line parameter λ to be of $O(Bo^{-2/3})$, and therefore define $\lambda = Bo^{-2/3}\lambda_0$, with $\lambda_0 = O(1)$ as $Bo \to 0$. Finally, we define the detuning parameter $\delta_0 = O(1)$ through

$$\omega = \omega_{2n-1}(1 + \delta_0 Bo^{2/3}).$$

In terms of these scaled variables and parameters, we must solve

$$\nabla^2\hat{\phi} = 0 \quad \text{for} \quad 0 \leqslant x \leqslant 1, \quad y \leqslant Bo^{1/3}\hat{\eta}(x,t), \tag{4.1}$$

subject to

$$\frac{\partial\hat{\phi}}{\partial x} = 0 \quad \text{at} \quad x = 0,1 \quad \text{for} \quad y \leqslant Bo^{1/3}\hat{\eta}(x,t), \tag{4.2}$$

$$\frac{\partial\hat{\phi}}{\partial t} + \tfrac{1}{2}Bo^{1/3}|\nabla\hat{\phi}|^2 = \frac{\partial^2\hat{\eta}}{\partial x^2}\left\{1 + Bo^{2/3}\left(\frac{\partial\hat{\eta}}{\partial x}\right)^2\right\}^{-3/2} + Bo^{2/3}(x - \tfrac{1}{2})\sin\omega t$$

$$\text{at} \quad y = Bo^{1/3}\hat{\eta}(x,t) \quad \text{for} \quad 0 \leqslant x \leqslant 1, \tag{4.3}$$

$$\frac{\partial\hat{\eta}}{\partial t} = \frac{\partial\hat{\phi}}{\partial y} - Bo^{1/3}\frac{\partial\hat{\phi}}{\partial x}\frac{\partial\hat{\eta}}{\partial x} \quad \text{at} \quad y = Bo^{1/3}\hat{\eta}(x,t) \quad \text{for} \quad 0 \leqslant x \leqslant 1, \tag{4.4}$$

$$|\nabla\hat{\phi}| \to 0 \quad \text{as} \quad y \to -\infty \quad \text{for} \quad 0 \leqslant x \leqslant 1, \tag{4.5}$$

$$\frac{\partial\hat{\eta}}{\partial x} = \begin{cases} Bo^{2/3}\dfrac{1}{\lambda_0}\dfrac{\partial\hat{\eta}}{\partial t} & \text{at} \quad x = 0, \quad y = Bo^{1/3}\hat{\eta}(0,t), \\ -Bo^{2/3}\dfrac{1}{\lambda_0}\dfrac{\partial\hat{\eta}}{\partial t} & \text{at} \quad x = 1, \quad y = Bo^{1/3}\hat{\eta}(1,t). \end{cases} \tag{4.6}$$

We now expand $\hat{\phi}$ and $\hat{\eta}$ as

$$\hat{\phi} = \hat{\phi}_0 + Bo^{1/3}\hat{\phi}_1 + Bo^{2/3}\hat{\phi}_2 + O(Bo), \quad \hat{\eta} = \hat{\eta}_0 + Bo^{1/3}\hat{\eta}_1 + Bo^{2/3}\hat{\eta}_2 + O(Bo),$$

and substitute into the governing equations. At leading order, assuming that the solution is driven by the forcing of $O(Bo^{2/3})$ that appears in (4.3), we obtain

$$\left.\begin{aligned}\hat{\phi}_0 &= \eta_{max}\frac{\omega}{(2n-1)\pi}\cos\omega(t-t_0)\cos(2n-1)\pi x\,\mathrm{e}^{(2n-1)\pi y},\\ \hat{\eta}_0 &= \eta_{max}\sin\omega(t-t_0)\cos(2n-1)\pi x,\end{aligned}\right\} \tag{4.7}$$

with η_{max} and t_0 constants that we will determine later using a secularity condition. Similarly, at $O(Bo^{1/3})$, we obtain

$$\left.\begin{aligned}\hat{\phi}_1 &= -\tfrac{1}{8}\eta_{max}^2\omega\sin 2\omega(t-t_0)\{1+2\cos 2(2n-1)\pi x\,\mathrm{e}^{2(2n-1)\pi y}\},\\ \hat{\eta}_1 &= \tfrac{1}{16}\eta_{max}^2(2n-1)\pi\{1+\cos 2\omega(t-t_0)\}\cos 2(2n-1)\pi x.\end{aligned}\right\} \tag{4.8}$$

Note that, because the leading-order term drives terms with twice the forcing frequency, there is no secularity condition at this order, and we must go to $O(Bo^{2/3})$.

After some tedious algebra, we arrive at the boundary value problem

$$\nabla^2\hat{\phi}_2 = 0 \quad \text{for} \quad 0\leqslant x\leqslant 1, \quad y\leqslant 0, \tag{4.9}$$

subject to

$$\frac{\partial\hat{\phi}_2}{\partial x} = 0 \quad \text{at} \quad x=0,1 \quad \text{for} \quad y\leqslant 0, \tag{4.10}$$

$$\frac{\partial\hat{\phi}_2}{\partial t} - \frac{\partial^2\hat{\eta}_2}{\partial x^2} = K_1\sin\omega(t-t_0)\cos(2n-1)\pi x + \text{non-secular}$$
$$\text{at} \quad y=0 \quad \text{for} \quad 0\leqslant x\leqslant 1, \tag{4.11}$$

$$\frac{\partial\hat{\eta}_2}{\partial t} - \frac{\partial\hat{\phi}_2}{\partial y} = K_2\cos\omega(t-t_0)\cos(2n-1)\pi x + \text{non-secular}$$
$$\text{at} \quad y=0 \quad \text{for} \quad 0\leqslant x\leqslant 1, \tag{4.12}$$

$$|\nabla\hat{\phi}_2| \to 0 \quad \text{as} \quad y\to-\infty \quad \text{for} \quad 0\leqslant x\leqslant 1, \tag{4.13}$$

$$\frac{\partial\hat{\eta}_2}{\partial x} = K_3\cos\omega(t-t_0) \quad \text{at} \quad x=0, y=0 \quad \text{and} \quad x=1, y=0, \tag{4.14}$$

where

$$K_1 = \tfrac{1}{2}\omega^2(2n-1)\pi\eta_{max}^3 + 2\delta_0(2n-1)^2\pi^2\eta_{max} - \frac{4}{(2n-1)^2\pi^2},$$

$$K_2 = -\tfrac{3}{32}(2n-1)^2\pi^2\omega\eta_{max}^3, \quad K_3 = \frac{1}{\lambda_0}\omega\eta_{max}.$$

If we now define the inner products of $\hat{\phi}_2$ and $\hat{\eta}_2$ with $\cos(2n-1)\pi x$ as

$$\bar{\eta}_2(t) = \int_0^1\hat{\eta}_2(x,t)\cos(2n-1)\pi x\,\mathrm{d}x, \quad \bar{\phi}_2(t) = \int_0^1\hat{\phi}_2(x,0,t)\cos(2n-1)\pi x\,\mathrm{d}x,$$

we find that the secular parts of the problem give

$$\frac{\mathrm{d}^2\bar{\eta}_2}{\mathrm{d}t^2} + \omega^2\bar{\eta}_2 = -2(2n-1)\pi K_3\cos\omega(t-t_0) + \tfrac{1}{2}\{(2n-1)\pi K_1 - \omega K_2\}\sin\omega(t-t_0), \tag{4.15}$$

$$\frac{\mathrm{d}^2\bar{\phi}_2}{\mathrm{d}t^2} + \omega^2\bar{\phi}_2 = -\tfrac{1}{2}\{(2n-1)^2\pi^2K_2 - \omega K_1\}\cos\omega(t-t_0) + 2\omega K_3\sin\omega(t-t_0). \tag{4.16}$$

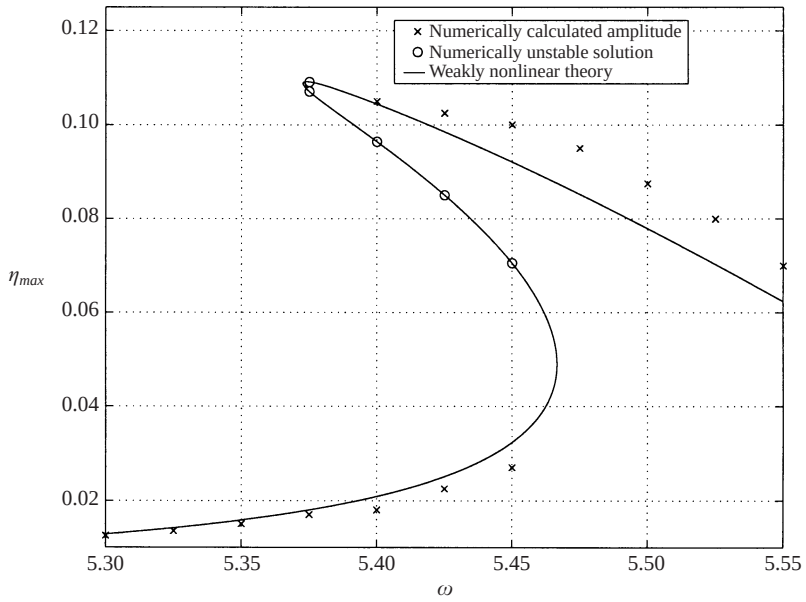

FIGURE 6. The response curve, calculated using (4.18), when $Bo = 0.03$ and $\lambda = 200$. The crosses indicate the amplitude of numerically calculated solutions, whilst circles indicate solutions that were unstable when used as initial conditions for numerical solutions. Note that $\omega_1 = \pi^{3/2} \approx 5.568$.

It is now straightforward to choose η_{max} and t_0 so that these secular terms are eliminated. We find that t_0, which represents the phase change between the response of the fluid and the external forcing, satisfies

$$\sin \omega t_0 = -\frac{1}{\lambda_0} \frac{\omega^3}{(2n-1)\pi} \eta_{max}, \tag{4.17}$$

whilst η_{max}, which gives the amplitude of the forced fluid motion, satisfies

$$\tfrac{19}{64}\omega^4 \eta_{max}^3 + (2n-1)\pi\omega^2 \delta_0 \eta_{max} - 2\sqrt{1 - \frac{\omega^4}{\lambda_0^2}(2n-1)\pi\eta_{max}^2} = 0. \tag{4.18}$$

This weakly nonlinear response is similar to that of a soft spring, whose elastic modulus decreases with deformation (see Ockendon & Ockendon 1973 for more on this). The resonant frequency of the system decreases as the amplitude of the forcing increases. Physically, the fluid that sloshes up the sides of the container takes longer to return towards the equilibrium position as the amplitude of the forcing increases and, in order to be synchronized with this fluid motion, the external forcing effectively has to wait for the fluid to move down the walls by decreasing its frequency. This effect can be seen clearly in the nonlinear solutions that we discuss in the next section.

A typical response curve is shown in figure 6. As is usual in systems of this type, there is the possibility of hysteresis. If the external frequency is higher than ω_{2n-1} and is slowly decreased, the amplitude of the response will follow the upper branch of the curve until it reaches the critical frequency at which the upper branch ends, when the amplitude of the response will drop onto the lower branch. If the forcing frequency is then slowly increased, the solution remains on the lower branch.

5. Numerical solution of the nonlinear, inviscid problem

Now that we have studied the behaviour of small-amplitude motions of the free surface, we turn to the problem of determining the behaviour when the lateral forcing is large enough that, at leading order, we must solve the fully nonlinear inviscid problem given by (2.1) to (2.8) with $Re^{-1} = 0$ and $\boldsymbol{u} = \nabla\phi$.

To solve the nonlinear free-surface problem, we adapt the desingularized integral equation technique described by Tuck (1997). This method seems to be more stable than the standard boundary integral technique, and in the following calculations no smoothing of the solution has been used. Beginning with the work of Cokelet & Longuet-Higgins (1976), who introduced a five-point smoothing formula, most numerical solutions of similar free-surface problems with surface tension have used some sort of smoothing to control grid-scale oscillations in the solution. A notable exception is the work of Hou, Lowengrub & Shelley (1994), who showed how to construct a semi-implicit numerical scheme by treating the stiff part of the governing equations implicitly. This allowed them to use a large number of points in their discretization without having to use a prohibitively small time step. An important observation made by Hou *et al.* is that, for fully explicit methods, the maximum possible timestep is controlled by the size of the smallest spatial separation in the discretization of the free surface. This has the unfortunate consequence that, the greater the required spatial resolution, even if it is localized in a small region of high surface curvature, the smaller the largest stable timestep.

5.1. *Numerical method*

We use a Lagrangian, time-explicit method to solve the boundary value problem given by (2.1)–(2.8) with $Re^{-1} = 0$ and $\boldsymbol{u} = \nabla\phi$. We solve for the position of $N+2$ points, (x_j, y_j) for $j = 0, 1, \ldots N+1$, initially equally spaced along the free surface. At all times, $x_0 = 0$ and $x_{N+1} = 1$, so that $j = 0$ and $j = N+1$ index the positions of the contact lines. We also solve for the velocity potential, Φ_j, at the other free-surface points, $j = 1, 2, \ldots N$. At the contact lines we can calculate the contact line velocity, $v_j = \partial\phi/\partial y(x_j, y_j)$ for $j = 0$ or $N+1$, by substituting a numerical approximation of the contact angle into (2.8).

5.1.1. *Solving Laplace's equation*

A solution of Laplace's equation that has no normal velocity at $x = 0$ and $x = 1$, and no flow as $y \to -\infty$ is

$$G_0(x, y) = \frac{1}{4\pi}\log(\sin^2 \tfrac{1}{2}\pi x + \sinh^2 \tfrac{1}{2}\pi y) + \tfrac{1}{4}y. \tag{5.1}$$

Between the walls, this has a single source of unit strength at $x = 0$, $y = 0$. By imaging this solution in $x = 0$, we obtain the Green's function

$$G(x, y; X, Y) = \begin{cases} G_0(x - X, y - Y) & \text{when} \quad X = 0 \text{ or } 1, \\ G_0(x - X, y - Y) + G_0(x + X, y - Y) & \text{when} \quad 0 < X < 1. \end{cases} \tag{5.2}$$

We can use this Green's function to construct an approximate solution of Laplace's equation by seeking a solution of the form

$$\phi(x, y) = \sum_{j=0}^{N+1} q_j G(x, y; X_j, Y_j), \tag{5.3}$$

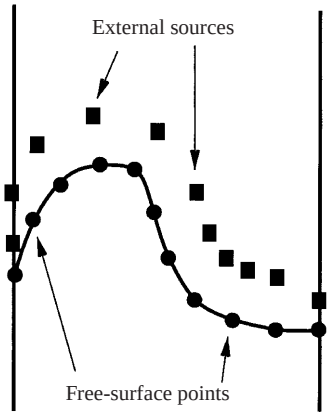

FIGURE 7. The discretization of the free surface and the associated point sources.

where (X_j, Y_j) are the positions of $N+2$ sources and q_j are their strengths. In essence, the boundary integral method uses $(x_j, y_j) = (X_j, Y_j)$, placing the sources at the free-surface points. In the desingularized integral equation method, which we choose to use here, each source point (X_j, Y_j) is placed outside the fluid. We place our sources a distance above the free surface equal to the average of the distance between (x_j, y_j) and the two adjacent free-surface points, in the normal direction at (x_j, y_j) for $j = 1, 2, \ldots N$, as shown in figure 7. If this results in a point lying outside the region between the walls, we simply move the point in the x-direction to lie on the wall. The sources associated with the two contact lines, $j = 0$, $N+1$, are each placed above the contact line a distance half the spacing between it and the adjacent free-surface point. A rigorous criterion for deciding the optimum placing of the sources is not known.

If we know ϕ at the free-surface points $j = 1, 2, \ldots N$ and $\partial\phi/\partial y$ at the contact lines, the source strengths, q_j, satisfy the linear equations

$$\sum_{j=0}^{N+1} A_{ij} q_j = B_i, \tag{5.4}$$

where

$$A_{ij} = \begin{cases} G(x_i, y_i; X_j, Y_j) & \text{for} \quad i = 1, 2, \ldots N, \\ (\partial G/\partial y)(x_i, y_i; X_j, Y_j) & \text{for} \quad i = 0 \text{ or } N+1, \end{cases} \tag{5.5}$$

$$B_i = \begin{cases} \Phi_i & \text{for} \quad i = 1, 2, \ldots N, \\ v_i & \text{for} \quad i = 0 \text{ or } N+1. \end{cases} \tag{5.6}$$

At each timestep we calculate the source strengths, q_j, by solving (5.4) using Gaussian elimination with partial pivoting. We can then calculate the velocity field at any point (x, y) using

$$u(x, y) = \sum_{j=0}^{N+1} q_j \frac{\partial G}{\partial x}(x, y; X_j, Y_j), \quad v(x, y) = \sum_{j=0}^{N+1} q_j \frac{\partial G}{\partial y}(x, y; X_j, Y_j). \tag{5.7}$$

In particular, we can find the velocity field at the $N+2$ free surface points. Note that the matrix A_{ij} is dense, asymmetric and not diagonally-dominant, so the solution of (5.4) by Gaussian elimination is the most inefficient and time-consuming step in this method.

5.1.2. *Timestepping*

Once we have an approximation to the velocity field, the simplest approach is to advect the free-surface points in this field, and update the velocity potential using the Bernoulli equation. However, this leads to the migration of points along the free surface, and hence to a non-uniform spacing. This is undesirable, firstly because it reduces the maximum timestep that we can take using an explicit method, as discussed above, and secondly because the discretization rapidly becomes unacceptably coarse along parts of the free surfaces. This second drawback is particularly acute for us, because the periodic, lateral forcing tends to drive the free-surface points into one half of the domain. We can overcome this by noting, as observed by Hou *et al.* (1994), that the tangential velocity of points in the free surface does not affect the flow. The limiting tangential velocity approaching the free surface from the bulk of the fluid is not necessarily equal to the tangential velocity of fluid particles actually on the free surface, since the flow is inviscid. This means that we can manipulate the tangential velocity in order to keep the spacing of the free-surface points fairly even, without affecting either the shape of the free surface or the velocity potential. With $\boldsymbol{u} = (u, v)$ the velocity field that we obtain by solving Laplace's equation, $\boldsymbol{n}_j$ the unit normal at the point (x_j, y_j) and $\boldsymbol{t}_j$ the unit tangent, both of which we can easily obtain from our approximation to the free surface, we choose to advect the jth free-surface point in the velocity field

$$\hat{\boldsymbol{u}}_j = (\boldsymbol{u} \cdot \boldsymbol{n}_j)\boldsymbol{n}_j + T_j \boldsymbol{t}_j. \tag{5.8}$$

We can now choose a form for the tangential velocity, T_j, that tends to keep the free-surface points fairly evenly spaced. We use

$$T_j = (N+1)^2(\mathrm{d}s_j - \mathrm{d}s_{j-1}), \tag{5.9}$$

with the distance between adjacent free-surface points given by

$$\mathrm{d}s_j = \sqrt{(x_{j+1} - x_j)^2 + (y_{j+1} - y_j)^2}. \tag{5.10}$$

This is equivalent to putting linear springs between neighbouring free-surface points. Comparisons between numerical solutions using this method and solutions advecting the free-surface points in the velocity field $\boldsymbol{u}$ are in good agreement, at least until the discretization in the latter solutions becomes too coarse to be reliable. We can think of (5.9) as diffusing away differences in point spacing.

The evolution equations for the x_j, y_j and Φ_j are

$$\frac{\mathrm{D}_j x_j}{\mathrm{D}t} = \hat{u}_j, \quad \frac{\mathrm{D}_j y_j}{\mathrm{D}t} = \hat{v}_j, \quad \frac{\mathrm{D}_j \Phi_j}{\mathrm{D}t} = \hat{\boldsymbol{u}} \cdot \boldsymbol{u} - \tfrac{1}{2}|\boldsymbol{u}|^2 + \kappa_j + Bo \sin \omega t \, x_j, \tag{5.11}$$

where

$$\frac{\mathrm{D}_j}{\mathrm{D}t} = \frac{\partial}{\partial t} + \hat{\boldsymbol{u}}_j \cdot \nabla,$$

and κ_j is the curvature of the free-surface at the jth free-surface point. We calculate κ_j, as well as the contact angles and the direction of the normal at each free-surface point using quartic splines. We integrated equations (5.11) using a second-order Runge–Kutta method, controlling the accuracy of the solution using a simple adaptive timestepping technique.

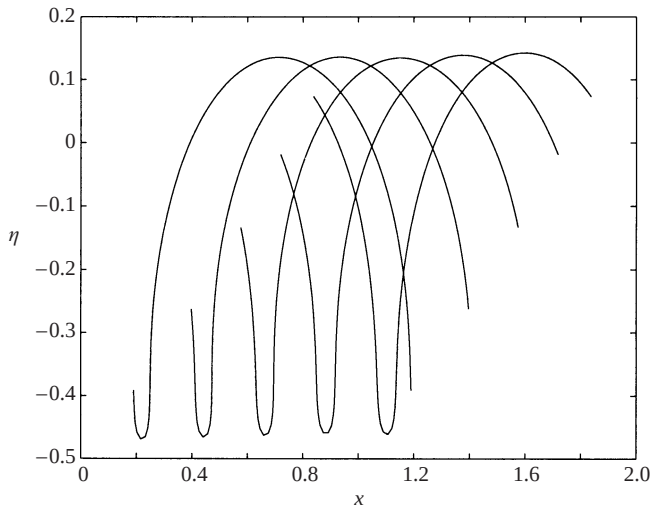

FIGURE 8. A numerical solution of the problem with periodic boundary conditions, shown at intervals of 0.1 time units, which correctly reproduces a solution found analytically by Crapper (1957).

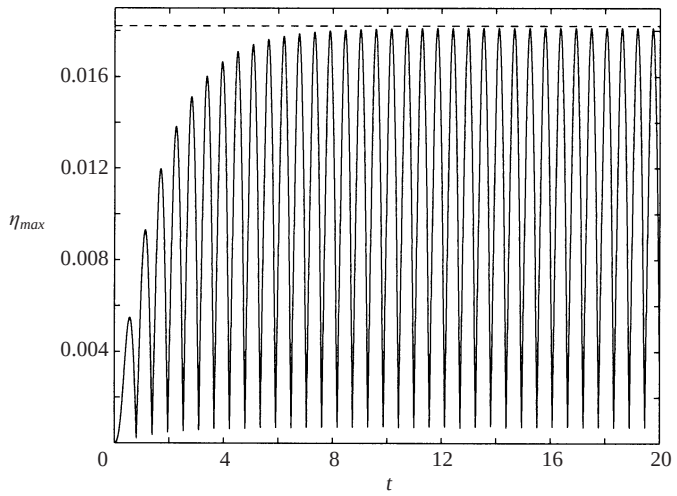

FIGURE 9. The maximum amplitude of the displacement of the free surface when $\lambda = 10$, $Bo = 0.1$ and $\omega = \pi^{3/2}$. The broken line indicates the amplitude predicted by the linear theory.

5.2. *Comparison of numerical and analytical solutions*

5.2.1. *Comparison with exact solutions for capillary waves*

As an initial test of this numerical method, we replace the contact lines with periodic boundary conditions and use as initial conditions the exact capillary wave solutions discovered by Crapper (1957). These propagate without change of form at a known speed. Numerical solutions, an example of which is shown in figure 8, correctly reproduce this behaviour.

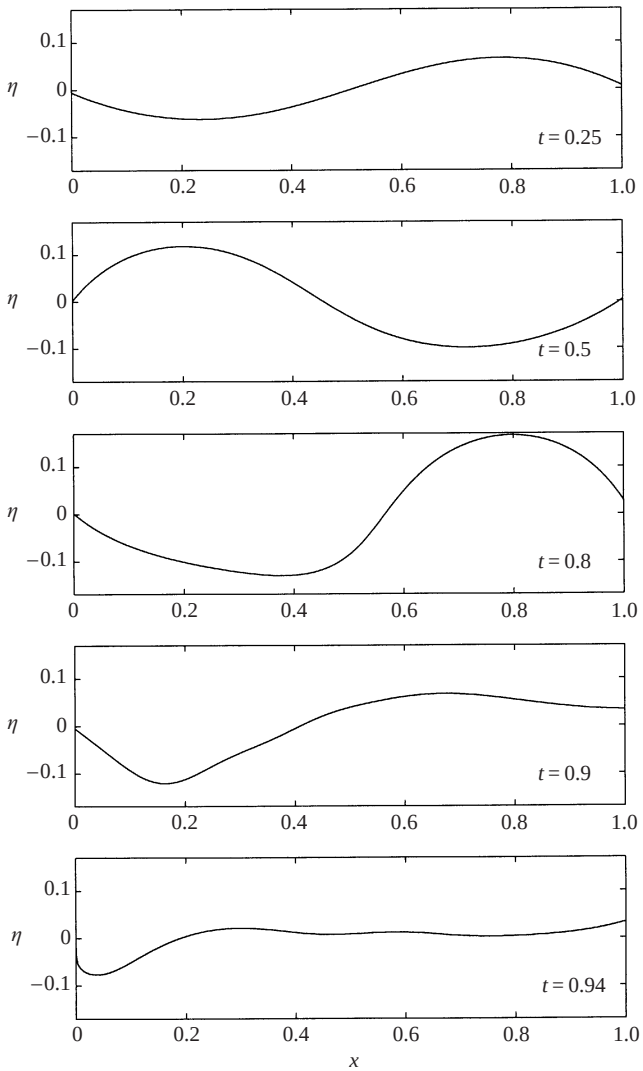

FIGURE 10. The solution when $\lambda = 0.1$, $\omega = 12.26$ and $Bo = 5$.

5.2.2. *Comparison with the linearized solution for small-amplitude forcing*

Starting from stationary initial conditions, the amplitude of the numerically calculated solution for forcing of small amplitude is, after the initial transients have decayed, always in excellent agreement with the analytical solution calculated in § 3. As an example, figure 9 shows the maximum amplitude of the displacement of the free surface when $\lambda = 10$, $Bo = 0.1$ and $\omega = \pi^{3/2}$, the resonant frequency for $\lambda = \infty$. The broken line indicates the amplitude predicted by the linear theory, and we can see that the agreement is excellent.

5.2.3. *Comparison with the weakly nonlinear solution for* $\lambda \gg 1$

In order to compare our numerical solutions with the weakly nonlinear analysis of § 4, we choose a typical case, $\lambda = 200$, $Bo = 0.03$, and use initial conditions consistent with the asymptotic solution for a range of values of ω and each possible value of

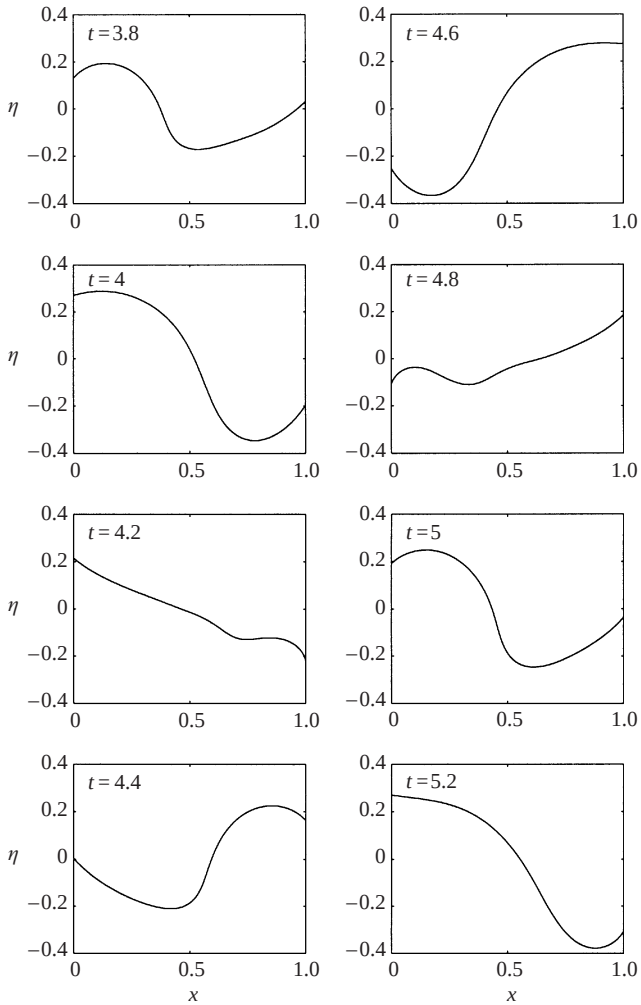

FIGURE 11. The solution when $\lambda = 1$, $\omega = \pi^{3/2}$ and $Bo = 10$.

η_{max}. We then let the solution settle down to a stable periodic solution, and record the maximum value of η. These are marked as crosses on figure 6. If the solution did not remain close to the solution predicted by the weakly nonlinear analysis, we concluded that the solution is unstable, and marked this with a circle in figure 6. These results are consistent with the asymptotic analysis.

These three test cases give us confidence that our numerical solution method is accurate, and we move on to study fully nonlinear solutions.

5.3. *Nonlinear numerical solutions*†

5.3.1. *Solutions with almost pinned contact lines* ($\lambda \ll 1$)

In numerical simulations with λ small, once Bo is large enough that the solution deviates significantly from the linearized solution, the contact angle starts to approach

† Mpeg movies of all of the following simulations can be obtained from http://for.mat.bham.ac.uk/J.Billingham/mpf.htm. These illustrate the results much more clearly than my attempts at describing them.

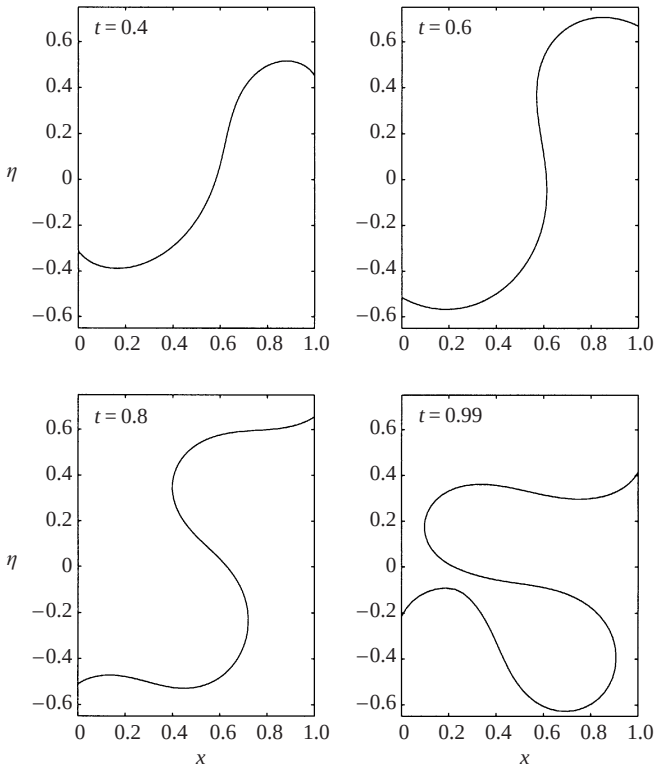

FIGURE 12. The solution when $\lambda = 1$, $\omega = \pi^{3/2}$ and $Bo = 20$.

π, at which point the simulation cannot be continued, since the numerical sources on the wall become too close to the free surface. A typical example is shown in figure 10.

5.3.2. *Solutions with* $\lambda = O(1)$

For moderately large values of Bo, a nonlinear periodic sloshing motion occurs. A typical example is shown in figure 11. For sufficiently large Bo, the fluid falls back on itself, a point beyond which we cannot continue the simulation, as shown in figure 12.

5.3.3. *Solutions with almost fixed contact angles* ($\lambda \gg 1$)

For moderate values of Bo, the motion of the fluid appears to be chaotic, as shown for a typical example in figure 13. Basically, the solution is similar to that shown for $\lambda = 1$ in figure 11, but with high-frequency, high-curvature transients superimposed. These regions of high curvature are similar to those found in previous studies of steady large-amplitude capillary and capillary–gravity waves. A close up of one such region is shown in figure 14, and should be compared to the highly curved region of the capillary wave shown in figure 8 and to figure 5 of Vanden-Broeck & Schwartz (1979).

For larger values of Bo, in contrast to the more highly damped motion when $\lambda = O(1)$, a region of the fluid pinches off at one of the walls, and the simulation can proceed no further. A typical example is shown in figure 15. Alternatively, the fluid may hit the opposite wall before pinch off occurs. For example, this occurs when $Bo = 18$, and the other parameters are unchanged from those used to produce figure 15.

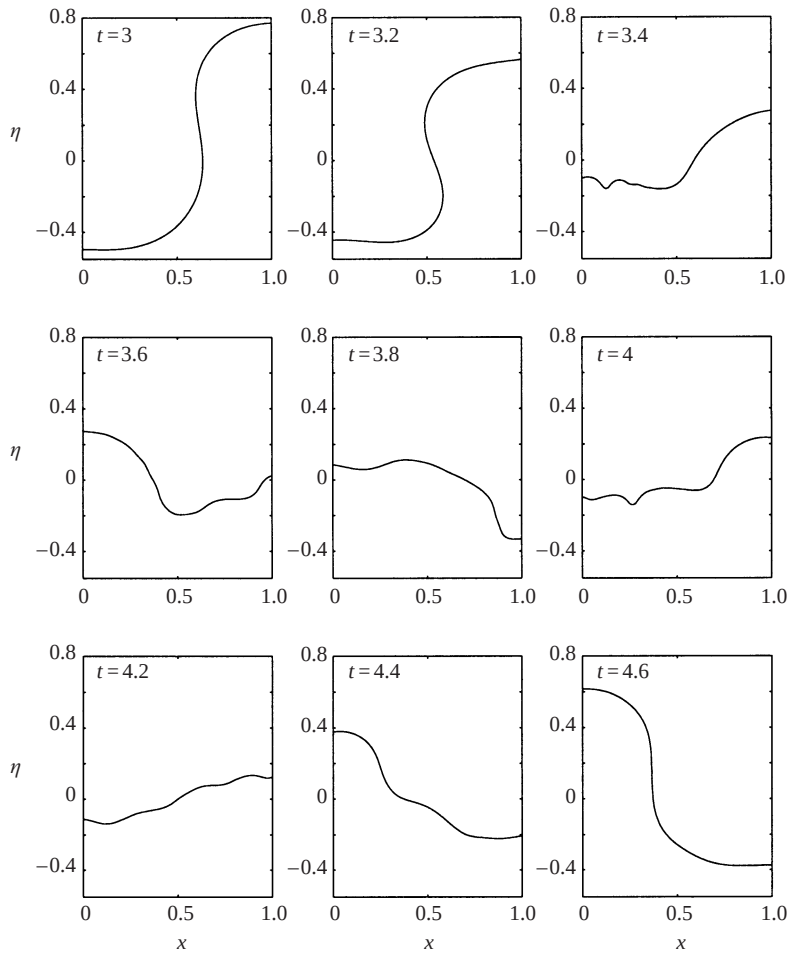

FIGURE 13. The solution when $\lambda = 10$, $\omega = \pi^{3/2}$ and $Bo = 10$.

6. Conclusions

In this paper we have considered a model problem, in which a fluid constrained by solid walls and moving contact lines is subjected to external forcing in the absence of gravity. After considering various analytical solutions, valid when the amplitude of the motion is sufficiently small, we studied the large-amplitude motion of the free surface using a desingularized integral equation technique. We found that the motion of the free surface, which can be periodic or chaotic, and can involve a change of topology, either through self-intersection or through pinch off at a wall, is crucially dependent on the behaviour of the contact angle as a function of contact line velocity.

The present investigation can be extended in a number of directions, which are currently being studied.

(i) The model we have used for the contact line is very simple, and may not be fully realistic. We aim to use instead the model proposed by Shikhmurzaev (1993) to determine how this affects the behaviour of the free surface.

(ii) The desingularized integral equation technique that we have used to solve the nonlinear inviscid problem is computationally very expensive, both because it involves inverting a full, unstructured matrix and because the problem is inherently

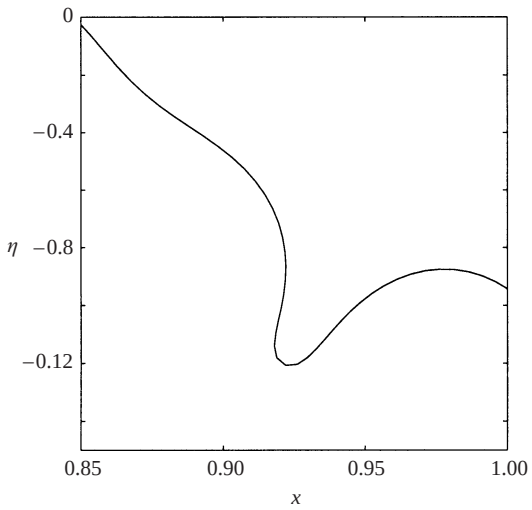

FIGURE 14. A close up of the solution when $\lambda = 10$, $\omega = \pi^{3/2}$, $Bo = 10$ and $t = 3.86$, showing a highly curved region.

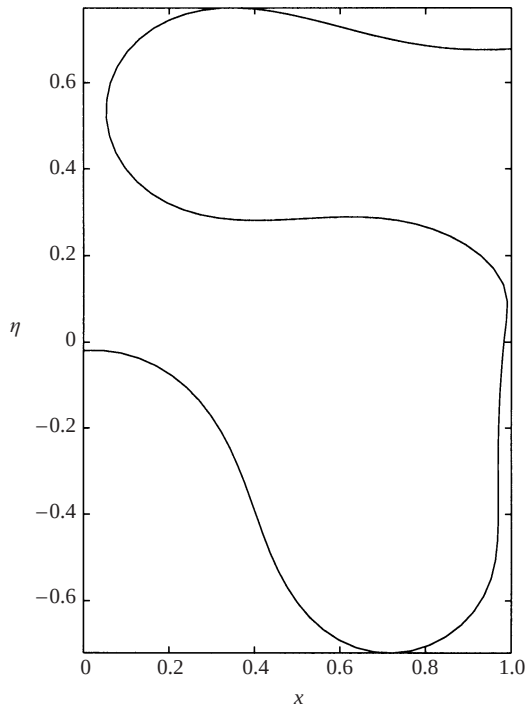

FIGURE 15. The solution as the fluid pinches off at the right-hand wall, when $\lambda = 10$, $\omega = \pi^{3/2}$ and $Bo = 16$ at $t = 1.15$.

very stiff. In order to overcome these problems, we plan to modify the semi-implicit method developed by Hou *et al.* (1994) to include contact lines. This would allow us much greater resolution of the free surface, since the method is computationally very efficient. In addition, this would open up the possibility of a simulation of the

three-dimensional version of this problem (for example, sloshing in a cylinder), which is completely out of reach using the desingularized integral equation method.

(iii) It is straightforward, although tedious, to include the effect of finite gravity in the analytical part of this work. In principle, it is also straightforward to include it in our numerical method. However, the need to resolve the capillary length scale, $\sqrt{\sigma/\rho g}$, rules out the use of the desingularized integral equation method, which is too computationally expensive.

(iv) We have neglected the effect of viscosity in our nonlinear simulations. Viscosity will act mainly in wall and surface boundary layers, and therefore our simulations underestimate the amount of damping that occurs. One approach to understanding this effect is to try to solve the associated boundary layer problems, including an appropriate model that eliminates the stress singularity at the moving contact line (Dussan V. & Davis 1974; Shikhmurzaev 1993). Another approach is to attempt a full Navier–Stokes simulation, as performed by Kamotani *et al.* (1995) and Wölk *et al.* (1997) for small-amplitude motions. The front-tracking method used by Popinet & Zaleski (1999) would be a sensible choice. Other possible methods are discussed in Scardovelli & Zaleski (1999).

I would like to thank Professor Ernie Tuck for suggesting this problem to me and allowing me to adapt his desingularized integral equation code to solve it, and also for his and his colleagues' hospitality at the University of Adelaide during my sabbatical in Australia. I would also like to thank the Royal Society for a travel grant, which made this collaboration possible.

REFERENCES

Billingham, J. & King, A. C. 1995 The interaction of a moving fluid/fluid interface with a flat plate. *J. Fluid Mech.* **296**, 325–351.

Cokelet, E. D. & Longuet-Higgins, M. S. 1976 The deformation of steep surface waves in water. A numerical method of computation. *Proc. R. Soc. Lond.* A **350**, 1–26.

Cox, R. G. 1986 The dynamics of spreading of liquids on a solid surface. Part 1. Viscous flow. *J. Fluid Mech.* **168**, 169–194.

Cox, R. G. 1998 Inertial and viscous effects on dynamic contact angles. *J. Fluid Mech.* **357**, 249–278.

Crapper, G. D. 1957 An exact solution for progressive capillary waves of arbitrary amplitude. *J. Fluid Mech.* **2**, 532–540.

Dreyer, M. E., Gerstmann, J., Stange, M., Rosendahl, U., Wölk, G. & Rath, H. J. 1998 Capillary effects under low gravity. *Space Forum* **3**, 87–136.

Dussan V., E. B. & Davis, S. H. 1974 On the motion of a fluid-fluid interface along a solid surface. *J. Fluid Mech.* **65**, 71–95.

Gerrits, J., Loots, G. E., Fekken, G. & Veldman, A. E. P. 1999 Liquid sloshing on earth and in space. In *Moving Boundaries V*, pp. 111–120. WIT Press, Southampton.

Gerrits, J. & Veldman, A. E. P. 2000 Numerical simulation of coupled liquid-solid dynamics. In *Proc. ECCOMAS 2000, Barcelona, paper* 575, http://www.math.rug.nl/veldman/preprints/ECCOMAS2000-GV. pdf.

Hocking, L. M. 1987 The damping of capillary-gravity waves at a rigid boundary. *J. Fluid Mech.* **179**, 253–266.

Hou, T. Y., Lowengrub, J. S. & Shelley, M. J. 1994 Removing the stiffness from interfacial flows with surface tension. *J. Comput. Phys.* **114**, 312–338.

Kamotani, Y., Chao, L., Ostrach, S. & Zhang, H. 1995 Effects of *g* jitter on free-surface motion in a cavity. *J. Spacecraft Rockets* **32**, 177–183.

Mei, C. C. & Liu, L. F. 1973 The damping of surface gravity waves in a bounded liquid. *J. Fluid Mech.* **59**, 239–256.

Ockendon, J. R. & Ockendon, H. 1973 Resonant surface waves. *J. Fluid Mech.* **59**, 397–413.

Ostrach, S. 1982 Low gravity fluid flows. *Annu. Rev. Fluid Mech.* **14**, 313–345.

Popinet, S. & Zaleski, S. 1999 A front-tracking algorithm for accurate representation of surface tension. *Intl J. Numer. Meth. Fluids* **30**, 775–793.

Scardovelli, R. & Zaleski, S. 1999 Direct numerical simulation of free-surface and interfacial flow. *Annu. Rev. F. Mech.* **31**, 567–603.

Shikhmurzaev, Y. D. 1993 The moving contact line on a smooth solid surface. *Int. J. Multiphase Flow* **19**, 589–610.

Tuck, E. O. 1997 Solution of free-surface problems by boundary and desingularised integral equation techniques. In *Computational Techniques and Applications: CTAC97*, World Scientific.

Vanden-Broeck J.-M. & Schwartz, L. W. 1979 Numerical solution of the exact equations for capillary-gravity waves. *J. Fluid Mech.* **95**, 119–139.

Weislogel, M. M. & Ross, H. D. 1990 Surface reorientation and settling in cylinders upon step reduction in gravity. *Microgravity Sci. and Tech.* **3**, 24–32.

Wölk, G., Dreyer, M., Rath, H. J. & Weislogel, M. M. 1997 Damped oscillations of a liquid/gas surface upon step reduction in gravity. *J. Spacecraft and Rockets* **34**, 110–117.